Using molecular imaging to assess the delivery and infection of protease activated virus in animal model of myocardial infarction

Banghe Zhu,[1] Caitlin Guenther,[2] Sunkuk Kwon,[1] Eva M. Sevick,[1]
and Junghae Suh[2]

[1]Center for Molecular Imaging, Brown Foundation Institute of Molecular Medicine, University of Texas Health Science Center, Houston, Texas, 77030
[2]Department of Bioengineering, Rice University, Houston, TX, 77005

ABSTRACT

Cardiovascular diseases remain the greatest cause of death in the US and gene therapy has the potential to be an effective therapy. In this study, we demonstrated MMP-9 based protease-activatable virus (PAV) for selective infection of myocardial infarct (MI) that is associated with active MMP-9 expression. To test the specificity of PAV, we used expression of a far-red fluorescence protein (iRFP) delivered by the PAV together with a dual PET/NIRF imaging agent specific for active MMP-9 activity at the site of MI in a murine model. Calibrated fluorescence imaging employed a highly-sensitive intensified camera, laser diode excitation sources, and filtration schemes based upon the spectra of iRFP and the NIRF agent. One to two days after ligation of the left anterior descending artery, the PAV or WT AAV9 virus encoding for iRFP (5×10^{10} genomic particles) and radiolabeled MMP-9 imaging agent (3 nmol) were injected intravenously (i.v.). PET imaging showed MMP activity was associated with adverse tissue remodeling at the site of the MI. One week after, animals were again injected i.v. with the MMP-9 agent (3 nmol) and 18-24 h later, the animals were euthanized and the hearts were harvested, sliced, and imaged for congruent iRFP transgene expression and NIRF signals associated with MMP-9 tissue activity. The fluorescent margins of iRFP and NIRF contrasted tissues were quantified in terms Standard International units of $mW/cm^2/sr$. The sensitivity, specificity, and accuracy of PAV and WT targeting to sites of MI was determined from these calibrated fluorescence measurements. The PAV demonstrated significantly higher delivery performance than that of the WT AAV9 virus.

Keywords: Molecular imaging, optical imaging, molecular and cellular imaging, gene therapy, cardiovascular disease, myocardial infarct, protease-activatable virus.

1. INTRODUCTION

Heart disease is the leading cause of death in the U.S. and close to 5 million Americans have heart failure [1]. Gene therapy has the potential to treat a number of cardiac diseases [2-3], with >150 gene therapy clinical trials worldwide for cardiovascular indications (J Gene Med database). Promisingly, there are a number of genes that could be delivered to treat post-myocardial infarction [4-6]. Unfortunately, many genes would have serious negative side effects if delivered systemically. Many promising therapeutic genes would only be clinically viable if they are delivered in a highly targeted manner to diseased cardiac tissues. Currently, specificity for target cardiac tissues is normally attempted through direct intramyocardial injection into a previously identified disease location or through the use of catheters to achieve localized delivery [7]. To decrease the invasiveness of current gene therapy approaches, delivery vectors need to be better targeted to cardiac tissues, enabling vectors to be injected intravenously (i.v.). Such an advancement should lead to the clinical translation of a greater number of gene/RNAi therapies for heart disease treatment.

The Suh lab at the Department of Biomedical Engineering at Rice University were the first to create adeno-associated virus (AAV) vectors that could be activated by extracellular proteases [8] that are biomarkers of tissue remodeling. Matrix metalloproteases -2 and -9 (MMP -2/-9) are gelatinases that are associated with adverse cardiac remodeling after myocardial infarct. The protease-activatable viral (PAV) vector is noninfectious in the absence of proteases but is then

able to "switch on" its cell surface receptor binding and cellular transduction behaviors upon exposure to specific MMPs. The PAV sensitivity and specificity can be tuned by modifying the amino acid sequence of the 'peptide lock' that we genetically incorporate into the capsid to build the vector.

Validation of *in vivo* AAV targeting and infection strategy depends upon quantitatively associating MMP activity with vector delivery and transgene expression. Use of far-red fluorescent protein (iRFP) represents a method to assess transgene expression in preclinical studies. While molecular imaging of MMP could provide an important companion diagnostic in clinical gene therapy trials that employ MMP targeted therapies, fluorescence-based techniques are not suited for the deep location of the heart in humans. Previously, we developed a dual-labeled imaging agent targeting active gelatinases (MMP -2/-9) for non-invasive, *in vivo* microPET/CT and NIRF imaging [9-10]. Herein, we use *in vivo* microPET/CT imaging of mice with induced myocardial infarct to detect MMP activity and *ex vivo* iRFP and NIRF fluorescence measurements calibrated in Standard International (SI) units for assessing accuracy of PAV targeting.

2. MATERIALS AND METHODS

2.1 AAV9-based PAV activated by MMPs and animal model of myocardial infract From a panel of MMP-activatable AAV9 vectors, one variant, L001 was selected with L001 having superior in vitro reactivity to both MMP-2 and MMP-9. To create a myocardial infarct, the left anterior descending artery (LAD) was ligated according to published procedures [11]. Two days after induction of the myocardial infarct, WT AAV9, L001 ($5x10^{10}$ genomic particles) were injected i.v. in 0.1 cc. One week later, the animals were anesthetized with isoflurane, administered 200 uCi of 18-FDG in 0.1 cc i.v., for microPET imaging 2 hours later to visualize the infarct. The following day, 200 uCi of 64-Cu-DOTA-IRDye800-MMP agent was administered in 0.1 cc i.v. for visualizing MMP activity in the infarct. Two weeks after PAV or AAV9 administration, animals were euthanized and the heart tissues collected for fluorescence imaging of iRFP transgene expression and NIRF-MMP activity.

2.2 MicroPET/CT Imaging
Animals were placed on a temperature-controlled pad at 37°C under isoflurane anesthesia. 70% isopropanol was used to clean the area at the site of injection (tail vein). Then an imaging agent was administered (i.v., <200 μL) before imaging. 18-F gated imaging was conducted immediately while 64-Cu non-gated imaging commenced more than 1 hour after agent administration. Imaging lasted no more than 45 minutes depending upon tissue activity and animals remained under isoflurane anesthesia during this time. Animals were allowed to recover and returned to the animal facility or at the last imaging session animals were euthanized and tissues collected.

2.3 iRFP and NIRF Imaging Instrumentation
Figure 1 provides the schematic of our fluorescence imaging system. A military-grade NIR sensitive Gen III image intensifier was employed to amplify the collected far red and NIRF light and convert it to a phosphor signal for registration in the optical green wavelengths by a frame-transfer 16-bit CCD camera. For iRFP imaging, an optically filtered diffused and broadened 690 nm laser diode was used to illuminate tissue surfaces with an incident power of around 1.0 mW/cm². iRFP fluorescent signals emanating from the animal were collected with two 720 nm band pass filters to increase the optical density at the excitation wavelength and reduce the excitation light leakage and improve sensitivity. For NIRF imaging, which has been previously described [12], we employed a 785 nm laser diode filtered with a "clean up" filter with an incident power of around 2.0 mW/cm². The collection of fluorescence signals was implemented by using two 830 nm band pass filters.
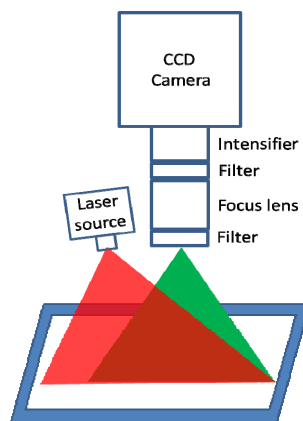
Fig.1. A schematic of the ICCD-based NIRF imaging system operating at two different wavelengths.

2.5 iRFP and NIRF Fluorescence Imaging

After 9 days post injection of PAV or WT AAV9, mice were sacrificed for *in situ* iRFP and NIRF fluorescence imaging. Then, the organs including hearts, brain, lung, liver, spleen and kidney were harvested for e*x vivo* both iRFP and NIRF fluorescence imaging. Finally, both iRFP and NIRF fluorescence imaging were performed on sliced hearts. During both iRFP and NIRF fluorescence imaging, the integrating time of CCD camera was set to 200 ms and the collected fluorescence signals were amplified by adjusting the gain of intensifier, but not exceeding the dynamic range of CCD camera (2^{16}). After both iRFP and NIRF fluorescence imaging, the sliced hearts were preserved in 10% formalin for pathological examination.

2.6 ROC Analysis for Assessing Tumor Margins from iRFP

A phantom with SI units of radiance was used to quantify the margin of iRFP contrasted tissues. NIRF images were thresholded to display intensities that were at least 1.86 times greater than that from negative tissues within the same field of view (FOV) and the margins were similarly extracted. The value of 1.86 was chosen as the minimum image contrast used for visual identification [13]. The boundary margin areas determined from iRFP and NIRF images were then calculated using ImageJ built-in functions. To assess the performance of the virus, we first compared the sensitivity of WT and PAV transfection in MMP denoted tissues. Sensitivity is defined as = area(MMP+/iRFP+)/(sum of areas (MMP+/IRFP+), (MMP+/IRFP-)). Next, we compared the specificity, i.e. how well WT and PAV targeted MMP+ tissues (or infarcted tissues). Specificity is defined as area (IRFP-/MMP-)/(sum of areas (IRFP-/MMP-), (IRFP+/MMP-)). Next we assessed the accuracy of WT versus PAV for targeting only MMP+ tissues (or infarcted tissues). Accuracy is defined as (sum of areas (IRP+/MMP+),(IRP-/MMP-))/(sum of areas (IRFP+/MMP+),(IRFP+/MMP-), (IRFP-/MMP+),(IRFP-/MMP-)). The statistical analysis was performed using the paired or unpaired Student's t-test, and Microsoft Office Excel 2010 software.

3. RESULTS

Figure 2(a) shows an example of the axial and coronal views of an 18-FGD gated PET/CT image with red arrows denoting non-viable, left ventricle heart tissues 2 weeks after LAD ligation. Figure 2(b) illustrates the infarcted heart 6 h after administration of 200 uCi of 64Cu-DOTA-IRDye800-MMP showing non-viable tissue uptake. In the nonviable tissue, a constant value of 2% of the injected dose/g (ID/gm) was found at 2, 6, and 24 h after administration. Note the MMP agent accumulates in the non-viable region in which there is no 18-FDG uptake.
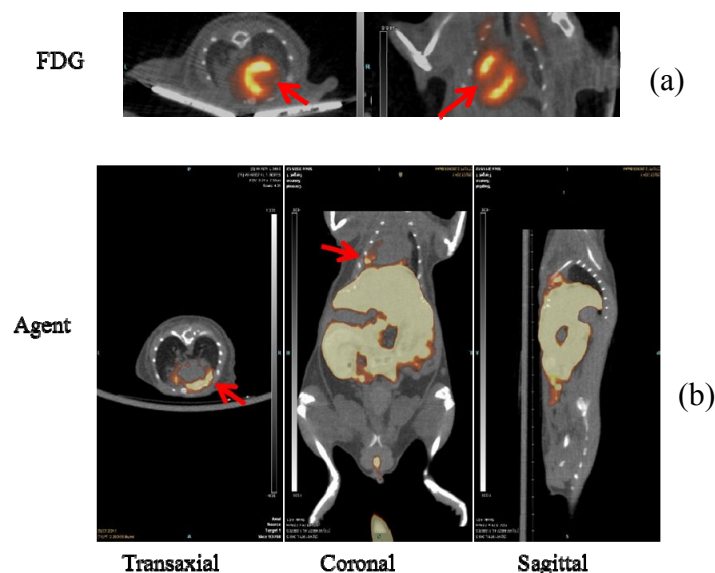
Fig.2. An infarcted heart contrasted by (a) FDG and (b) [64] Cu-DOTA-IRDye 800-MMP imaging agent. FDG images were acquired using gating on EKG.

To validate the fluorescence methodology for assessing iRFP transgene expression, WT AAV9 carrying iRFP was administered in normal healthy animals with expected non-specific uptake in the heart and in the liver. As shown in Figure 3, 2 and 3 weeks after AAV9 administration, the iRFP expression in the liver and heart could be detected above autofluorescence levels *in situ*, and expression was easily detected *ex vivo* using the iRFP imaging system. We also validated iRFP mRNA expression using qPCR (not shown for brevity) If the PAV is effective, they should show decreased iRFP transgene expression in the normal healthy animals and only in the hearts of animals with myocardial infarcts.
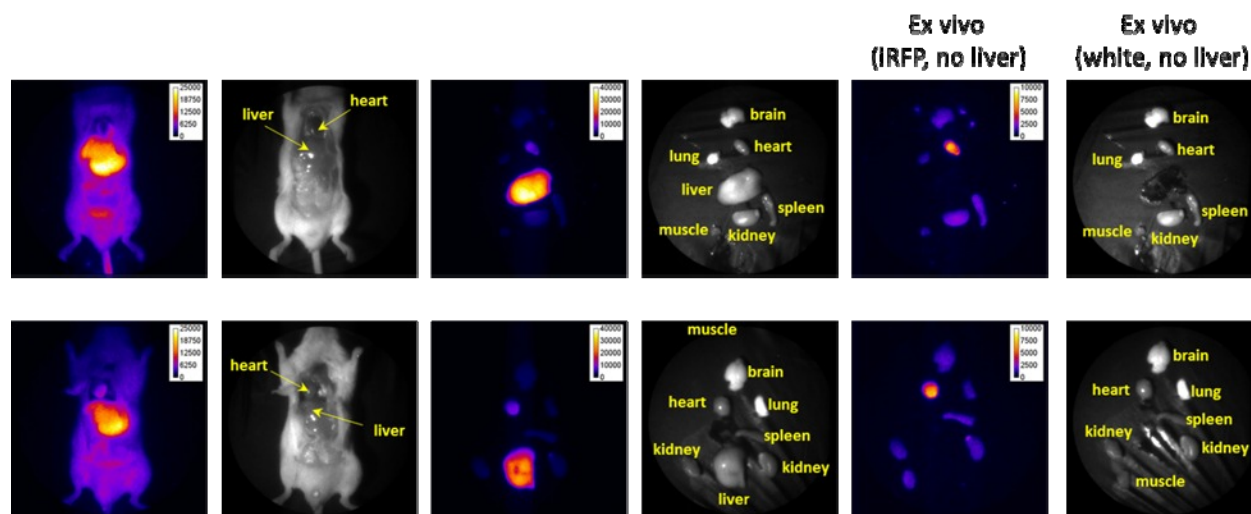

Fig.3. *In situ* and *ex vivo* iRFP fluorescence images reveal the PAV delivery of iRFP associated with the MMPs in the infarcted heart.

Figure 4 shows the extracted margins of the typical *ex vivo* iRFP, and NIRF images of an infarcted, sliced heart. The calculated sensitivity, specificity and accuracy are shown in Figure 5. As expected, L001 and WT AAV9 show equally high sensitivity since AAV9 tends to accumulate throughout the heart, but L001 is superior in specificity to infarcted tissues than WT AAV9, further evidence of the PAV mode of transduction *in vivo*. There is no statistical difference between L001 and WT AAV9 in sensitivity. There is a statistical difference between L001 and WT AAV9 in specificity and accuracy.
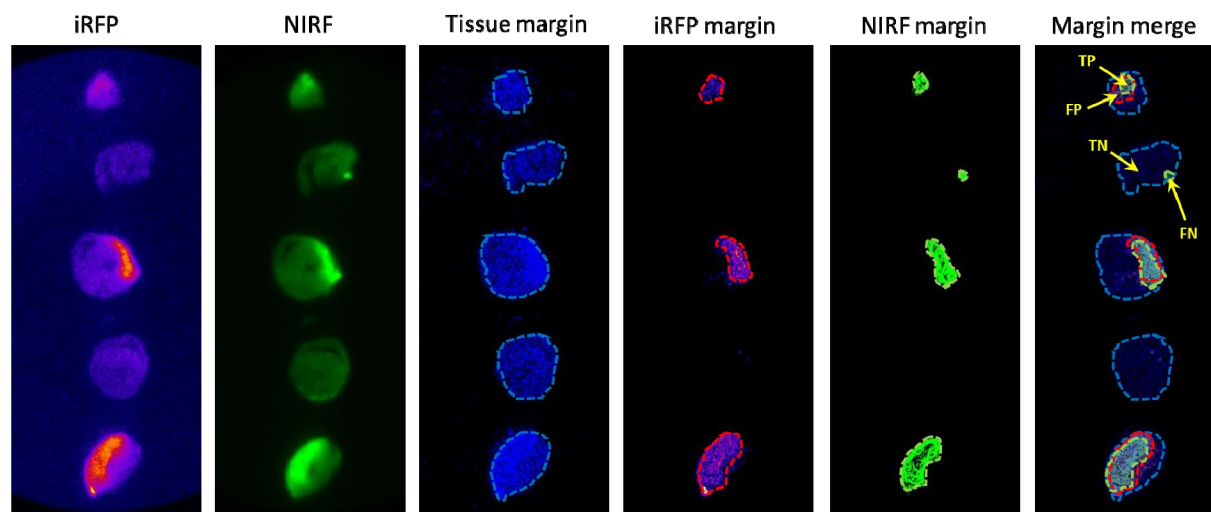

Fig.4. The margins of a representative sliced heart determined by boundary analyses of iRFP, NIRF signals, and their overlays. The margins denoted by the iRFP threshold found by phantom and by NIRF contrast of 1.86 are denoted on the image.
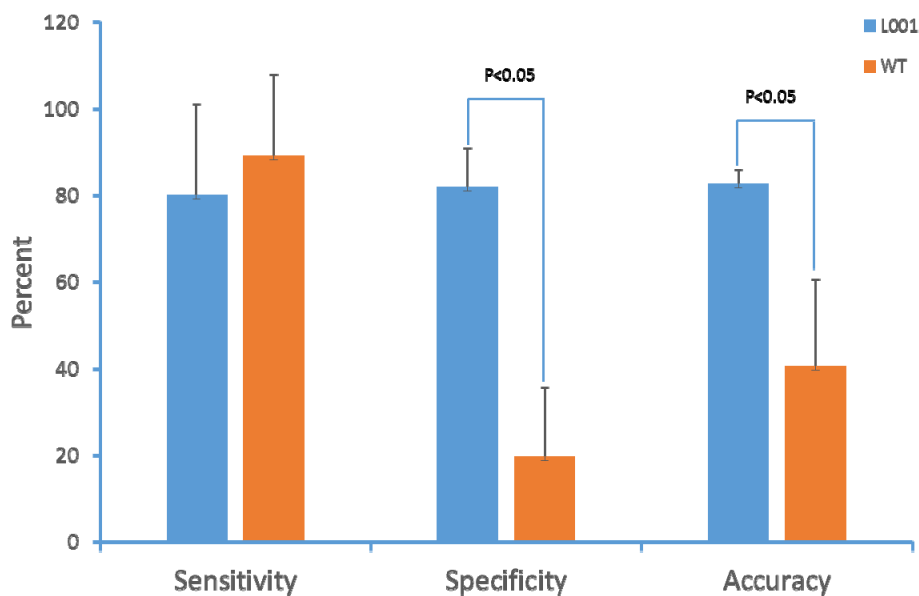

Fig.5. The sensitivity, specificity and accuracy of PAV and WT targeting to sites of MI, demonstrating significantly higher delivery performance of PAV compared to WT AAV9 virus.

4. SUMMARY

Vectors with specificity to damaged heart tissues would be an advancement towards achieving effective cardiac gene therapies. In this study, PAV was designed to be activated by MMP-9, a tissue marker of myocardial infarction. To test the delivery performance of PAV, iRFP far-red fluorescence protein (iRFP) transgene expression was correlated to MMP-9 activity as measured with a dual labeled, PET and NIRF labeled targeted peptide. The results show that the accuracy for targeting infarcted tissues is 78% compared to the 6% accuracy of that of WT AAV9 virus (78% vs 6 %).

ACKNOWLEDGEMENTS

REFERENCES

[1]   Roger V. L., Go A. S., Lloyd-Jones D. M., et al, "Heart disease and stroke statistics--2012 update: a report from the American Heart Association," Circulation. 125(1):e2-e220 (2012).

[2]   Chaanine A. H., Kalman J., Hajjar R. J., "Cardiac gene therapy," Seminars in Thoracic and Cardiovascular Surgery. 22(2):127-139 (2010).

[3]   Pacak C. A., Byrne B. J., "AAV Vectors for Cardiac Gene Transfer: Experimental Tools and Clinical Opportunities. Molecular Therapy," 19(9):1582-1590 (2011).

[4]   Fedak P. W., Smookler D. S., Kassiri Z., et al, "TIMP-3 deficiency leads to dilated cardiomyopathy," Circulation. 110(16):2401-2409 (2004).

[5]   Fedak P. W., Altamentova S. M., Weisel R. D., et al, "Matrix remodeling in experimental and human heart failure: a possible regulatory role for TIMP-3," American journal of physiology Heart and Circulatory Physiology. 284(2):H626-634 (2003).

[6]   Tian H., Cimini M., Fedak P.W., et al, "TIMP-3 deficiency accelerates cardiac remodeling after myocardial infarction," Journal of Molecular and Cellular Cardiology. 43(6):733-743 (2007).

[7]   Tilemann L., Ishikawa K., Weber T., Hajjar R. J., "Gene Therapy for Heart Failure," Circulation Research. 110(5):777-793 (2012).

[8]   Judd J., Ho M. L., Tiwari A., et al, "Tunable protease-activatable virus nanonodes," ACS Nano. 8(5):4740-4746 (2014).

[9]   Rodenberg E., Azhdarinia A., Lazard Z. W., et al, "Matrix metalloproteinase-9 is a diagnostic marker of heterotopic ossification in a murine model," Tissue Engineering Part A. 17(19-20):2487-2496 (2011).

[10]   Azhdarinia A., Wilganowski N., Robinson H., et al, "Characterization of chemical, radiochemical and optical properties of a dual-labeled MMP-9 targeting peptide," Bioorganic & Medicinal Chemistry. 19(12):3769-3776 (2011).

[11]   Kolk M. V., Meyberg D., Deuse T., et al, "LAD-ligation: a murine model of myocardial infarction," Journal of visualized experiments : JoVE. (32) (2009).

[12]   Zhu B., Rasmussen J. C., Lu Y., Sevick-Muraca E. M., "Reduction of excitation light leakage to improve near-infrared fluorescence imaging for tissue surface and deep tissue imaging," Medical Physics. 37(11):5961-5970 (2010).

[13]   Murthy K., Aznar M., Thompson C. J., Loutfi A., Lisbona R., Gagnon J. H., "Results of preliminary clinical trials of the positron emission mammography system PEM-I: a dedicated breast imaging system producing glucose metabolic images using FDG," Journal of Nuclear Medicine. 41(11):1851-1858 (2000).